ELSEVIER

Journal of Alloys and Compounds 228 (1995) 188–194

Journal of ALLOYS AND COMPOUNDS

Short-range order of yttria doped zirconia powders study by X-ray absorption (I)

C. Jiménez-Solís[a], L. Esquivias[a], C. Prieto[b]

[a]*Departamento de Física de la Materia Condensada, Facultad de Ciencias, Universidad de Cádiz, Apartado 40, Puerto Real, 11510 Cádiz, Spain*

[b]*Instituto de Ciencias de Materiales de Madrid, Consejo Superior de Investigaciones Científicas, Facultad de Ciencias, Universidad Autónoma, 28049 Madrid, Spain*

Received 14 April 1995; in final form 12 May 1995

Abstract

The atomic structure of polymorphic zirconia powders doped with yttria 6 mol% prepared from $ZrOCl_2 \cdot 8H_2O$ and Y_2O_3 has been studied by X-ray absorption spectroscopy. The short-range orders before and after heat treatment have been compared. The crystallization and incorporation of the yttrium atoms to the network have been monitored.

Keywords: Zirconia; X-ray absorption; XANES; EXAFS

1. Introduction

Pure zirconia is polymorphic. At normal pressure it can be found in monoclinic (room temperature), tetragonal (1100–2360°C) and cubic (2360–2600°C) phases. They are abbreviated as m-, t- and c-ZrO_2 herein. Nevertheless, tetragonal and cubic phases can be formed at room temperature by adding adequate amounts of oxides of metals with similar atomic radii, like yttrium. The tetragonal phase is metastable (it can be transformed into monoclinic by a temperature change or a stress field) but the cubic phase is stable. Thus, the material is said to be fully or partially stabilized according to the percentage of cubic phase. The excellent mechanical properties of these materials arise from the stress induced during the transformation from the tetragonal to the less dense monoclinic phase. When this transformation is caused by the stress field around a crack (martensitic transformation), the volume increase of transformed crystallites prevents crack propagation. Not only are the structural properties of zirconia-based ceramics remarkable, but functional advantages can also be drawn from these materials in applications such as oxygen sensors, coatings, electrolytes, etc. [1–6]. This has given rise to extensive research, the common aims of which are obtaining high purity, nano-sized and sinterable particles to prepare high density ceramics [7–15] as well as in-depth studies of their physical and chemical properties [16,17].

The techniques employed up to now to prepare fine powders of stabilized ZrO_2 are quite numerous: co-precipitation of inorganic aqueous solution by pH control [8], thermal decomposition and hydrolysis of metallic alkoxides [9], hydrothermal reaction at high pressure [12], forced hydrolysis of highly-acidic metallic salts solutions [13,14]. The actual distribution of the dopants depends on the method. In some cases, the stabilizing oxide is added just before calcination and then, by diffusion, the dopant is uniformly dispersed. As a consequence, this involves an increase of the particle size with the subsequent lowering of the sinterability of powders.

A major problem occurs in the processing of multi-component-ceramic-powders: to find a method that guarantees homogeneity at a molecular level. The sol–gel technique from alkoxides [9] is plausible to obtain powders with a high degree of chemical homogeneity. High purity and easy sintering will result if a total elimination of the unwanted organic residues has been previously completed. However, high cost is a major inconvenience attributed to this method. Hydrolysis of salts is a less expensive alternative. Only remarkable differences in the performance of products

SSDI 0925-8388(95)01883-2

prepared by the first method would make its use advisable.

Extended X-ray absorption fine structure (EXAFS) is a powerful probe that allows the structural characterization around a localized atomic species, even in very diluted cases. Owing to its selectivity, if the short-range orders of the involved species are different enough, it can be used to study the homogeneity of the material at an atomic level. This can be done with the Fourier transform (FT) of the EXAFS function, which gives a qualitative radial distribution function around an arbitrary atom.

Recently, Ping-Li et al. [18–20] have published a complete work on X-ray absorption of zirconia powders prepared by coprecipitation of Y and Zr salts. They reported clear results of each polymorph individually treated. Their results show that the Zr–O bonding is similar in m-, o- and c-Zr with sevenfold coordination and comparable bond distances. Consequently, the Zr-cation network in c-ZrO_2 is very distorted to accommodate the sevenfold Zr–O polyhedra. In the present paper, results are given on a polymorphic sample in which all the polymorphs coexist. EXAFS analysis is used here as a tool to study the sample inhomogeneity and the local order rearrangement caused by crystallization rather than the polymorph structures. In a forthcoming paper the X-ray absorption of yttria doped zirconia powders prepared by alkoxide hydrolysis will be discussed.

2. Experimental procedures

2.1. Powders preparation

$ZrOCl_2 \cdot 8H_2O$ was dissolved with the minimum amount of water allowing its total dissolution. Next, an adequate amount of yttria was dissolved in 0.1 N HCl to give 6 mol% of yttria doped zirconia as final product. Both solutions were mixed and sonicated for 8 s g^{-1}. NH_4OH was added to this mixture until it attained pH = 9. The resultant colloid was filtered and washed with ethanol several times. Then, it was dried at 80°C and milled in ethanol.

Once dried, the powder was heated at 350°C for 16 h with a heating rate of 1°C min^{-1}. Next, the powder was heat treated at 600°C for 2 h.

Samples are referred as xC, where $x = 1$ indicates as-prepared and $x = 2$ indicates heat treated at 600°C.

2.2. Acquiring and analyzing X-ray absorption near edge structure (XANES) and EXAFS data

Experiments were carried out on the beam line XAS3 at D.C.I. storage ring (Orsay, France) with an electron beam energy of 1.85 GeV and an average current of 250 mA. Data were collected with a fixed exit monochromator using two flat Si (311) crystals in transmission mode. Detection was made using two ion chambers with air as the filled gas and a photomultiplier with a scintillation plastic for the fluorescence yield detection. The fast-EXAFS-acquisition operative mode [21] was used to collect at least ten spectra in a limited time with sufficient signal-to-noise ratio. Energy resolution was estimated to be about 2 eV from the Cu foil 3d near edge feature. The energy calibration was monitored using the Cu foil sample and was set at 8991 eV at the first maximum of the derivative spectrum. EXAFS spectra were performed over a range of 800 eV above the Zr and Y K-edge of samples 1C and 2C.

A conventional procedure [22] has been used to analyze the EXAFS spectrum at a given X-ray energy E, $\chi(k)$, where $k = [(2m_e/\hbar^2)(E - E_0)]^{1/2}$ is the photoelectron wave vector modulus, m_e being the electron mass and E_0 the threshold energy. As usual, an approximate energy value near the edge (E_{0i}) was initially assigned to $k = 0$. Then, during fitting, $\Delta E_0 = E_0 - E_{0i}$ is treated as an additional parameter.

To evaluate the neighbor's position around the absorber atoms, the well-known theoretical EXAFS function was used:

$$\chi(k) = \sum_j \frac{N_j}{kR_j^2} \exp(-2k^2\sigma_j^2) \exp\left(\frac{\Gamma_j R_j}{k}\right) f_j \sin[2kR_j + \psi_j(k)] \quad (1)$$

This expression describes the EXAFS oscillations for a Gaussian distribution of neighbors around the absorber atom, in the single scattering theory and in the plane-wave approximation. N_j is the average coordination number for the Gaussian distribution of distances centered at R_j; σ_j is the Debye–Waller contribution; $\psi_j = 2\delta(k) + \gamma_j(k)$ is the phase shift, $\delta(k)$ and $\gamma_j(k)$ respectively being that of the central and backscattering atoms; f_j is the amplitude of the backscattering atoms; $\Gamma_j = k/\Lambda(k)$, $\Lambda(k)$ being the photoelectron mean free path.

The FT of $k^3\chi(k)$ is the pseudo radial distribution function (PRDF). This transform is related to the radial distribution of atoms surrounding the Zr or Y atoms with a shift caused by the scattering phase [23]. $f_j(k)$ and $\psi_j(k)$ have been theoretically calculated by the method reported by Rehr et al. [24] which includes a calculation of $\Lambda(k)$. To avoid spurious oscillations, FTs were calculated with a Hanning window selecting the transform range from 3–11 Å above the edge.

An FT^{-1} filtering was used to extract the EXAFS contribution of the first coordination sphere, supposed to be monolayer (only O atoms around Zr or Y). This results in the isolation of the Zr–O or Y–O shell contribution in $k^3\chi(k)$. Data have been fitted in the k-

and R-spaces by comparison of experimental data filtered and spectra calculated by Eq. (1). After this process, a least squares method has been applied in order to obtain the parameters. With the aim of reducing the number of EXAFS parameters or to test the resulting values, we have initially used the reported structural parameters [25–32]. A two-shell or three-shell model is reported only if this gives a much better fit than the single distance fitting.

For all the XANES spectra, a Victoreen law, extrapolated from the low energy, has been subtracted and the normalization performed. Their interpretation was qualitatively made on the basis of empirical ideas.

Phase identification was made by X-ray diffraction (XRD) using Cu Kα radiation ($\lambda = 1.542$ Å).

3. Results

The XANES spectra are represented in Fig. 1 and their first derivative in Fig. 2. A small shoulder at about 10 eV from the edge threshold in Fig. 1, and its counterpart peak in Fig. 2, are observed in the Zr K-edge spectrum of 2C. This has been attributed to a $1s \rightarrow 4d$ transition that is enhanced by tetrahedral geometry [33]. The sample spectrum of 1C does not show such a feature. Another feature is a splitting of the main peak, easily located in the first derivative plot. This splitting is more striking as the content of Y_2O_3 increases [19]. Furthermore, a third feature located 30 eV after the edge has also been observed which increases with Y concentration [18].

Similar XANES spectra at Y K-edge are observed in calcined and as-prepared samples. Differences are observed at energies 40 eV higher than the absorption threshold. These are probably structure dependent features, and are very difficult to interpret due to the complicated multiple scattering process expected to occur at this energy range.

Different local order around Zr and Y atoms is immediately inferred from the shape, amplitude and frequency of the EXAFS spectra Zr and Y K-edges, shown in Fig. 3. Fig. 4 illustrates the FT of $k^3\chi(k)$ signals of powders of samples 1C and 2C. The fits

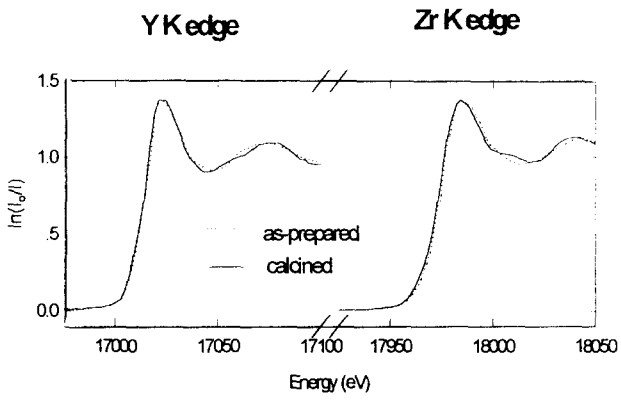

Fig. 1. Y K-edge (left) and Zr K-edge (right) room temperature XANES spectra of the zirconia powders doped with yttria 6 mol%.

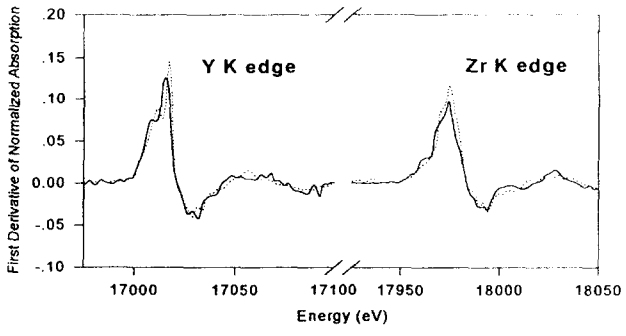

Fig. 2. First derivative of Y and Zr XANES for as-prepared (dotted line) and calcined (continuous line) zirconia powders doped with yttria 6 mol%.

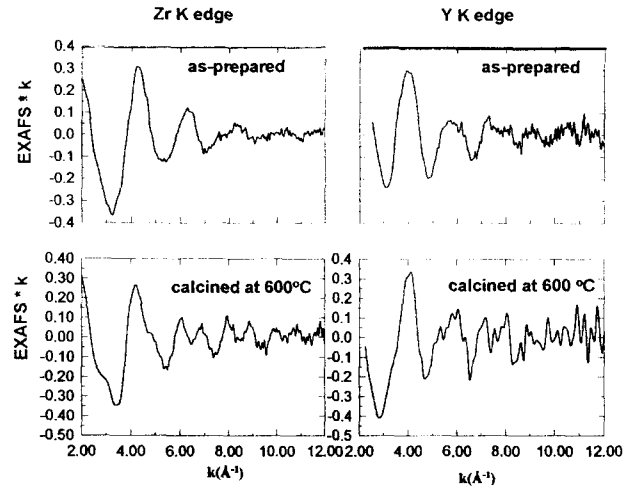

Fig. 3. Room temperature EXAFS spectra of Zr K-edge (left) and Y K-edge (right) for as-prepared (top) and calcined (bottom) zirconia powders doped with yttria at 6 mol%.

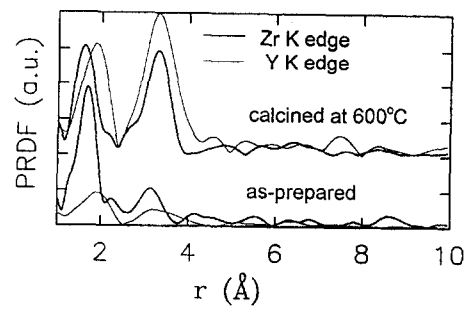

Fig. 4. Fourier transform of Zr and Y k^3EXAFS weighted signals for as-prepared (bottom) and calcined (top) zirconia powders doped with yttria at 6 mol %.

obtained in the real space are represented in Figs. 5 and 6. Table 1 lists the values used in Fourier filtering and the structural data resulting from the fitting.

For the fitting we have supposed, from Shannon's table of ionic radii [33], that Zr–O bond length in the amorphous sample is 2.22 Å. Since the interatomic distances are highly correlated to ΔE_0, the R_j value, once N_{CN} is fixed at a reasonable integer, was used to obtain the best fit to the experimental data of 1C and 2C samples. Then, R_j and σ_j is allowed to float up to obtain a good fitting. For analysis of cation–cation scattering, as Zr or Y have nearly the same scattering behavior we have considered them to be indiscernible. Thus, the Zr-cation shell was fitted without allowing for differences between Zr and Y as second nearest neighbors. We have taken 12 as the coordination number and 3.62 Å as the Zr-cation distance. The fitting was considerably improved with a two-shell

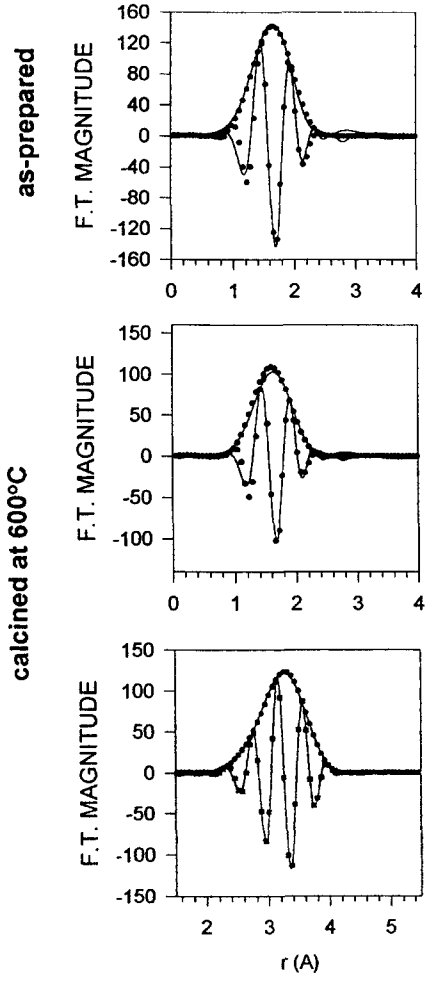

Fig. 5. Comparison of experimental (points) with calculated (continuous line) modulus and imaginary part of the filtered EXAFS data in R-space at Zr K-edge for Zr–O shell of the as-prepared sample (top), Zr–O shell of the calcined sample (middle) and Zr-cation shell of the calcined sample (bottom).

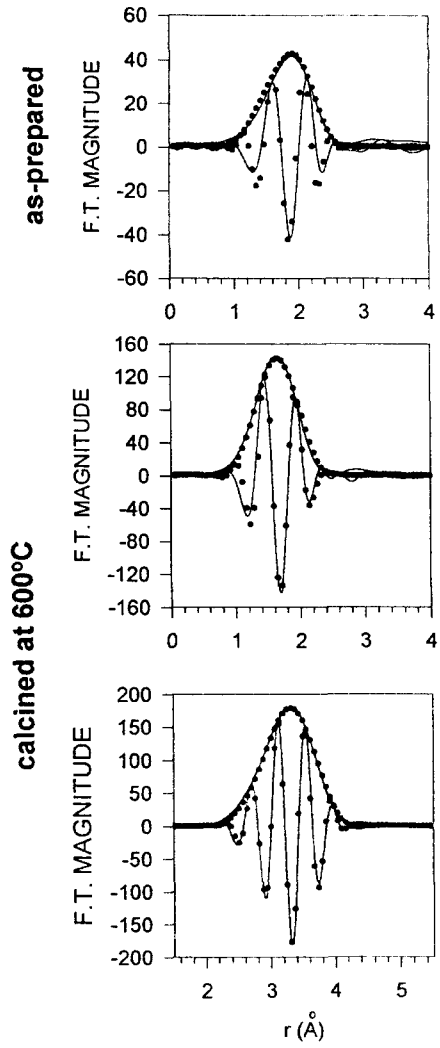

Fig. 6. Comparison of experimental (points) with calculated (continuous line) modulus and imaginary part of the filtered EXAFS data in R-space at Y K-edge for Y–O shell of the as-prepared sample (top), Y–O shell of the calcined sample (middle) and Y-cation shell of the calcined sample (bottom).

model. Several integer coordination numbers were tested during the refinement of R_2 and σ_2.

For the fitting of the filtered nearest neighbor signals of the Y K-edge $k^3\chi(k)$, a similar procedure was followed. The starting values of the nearest neighbors' distance and coordination numbers were those of Y–O in Y_2O_3 (6×2.28 Å). However, the frequency of the 1C EXAFS function, that is R_1, was substantially higher and replaced by 2.44 Å, that is the value reported of the Y–OH bond in $Y(OH)_3$ [32]. The ΔE_0, σ_1 and R_1 were refined with $\sigma = 0.1$ Å^{-1} as start value. Once a rough fitting was obtained, small variations of σ_1 and R_1 were allowed for a given reasonable N_{CN} to obtain the best fitting. As the resulting R_1 is quite different from those reported in Refs. [19,20], several window functions were examined (Fig. 7). By changing

Table 1
EXAFS result of zirconia powders doped with yttria at 6 mol%

Edge	Sample	Bonding	ΔR (Å)	Δk (Å)	N_{cn}	R (Å)	σ^2 (Å^2)	ΔE_0 (eV)	ε^a (%)
Zr	as-prepared	Zr–O	1.1–2.1	3.0–11.0	8	2.22	0.0116	−10	8.7
	calcined	Zr–O	1.2–2.0	3.0–11.0	4	2.18	0.0077	−10	22.1
	calcined	Zr-cation	2.4–3.9	3.0–11.0	10	3.62	0.0102	8.7	9.0
					2	3.75			
Y	as-prepared	Y–O	1.2–2.5	3.0–11.0	6	2.56	0.0205	−10	65.3
	calcined	Y–O	1.2–2.4	3.0–11.0	6	2.51	0.0056	−0.6	15.4
					2	2.33	0.0056		
	calcined	Y-cation	2.4–4.2	3.0–11.0	6	3.55	0.0045	−0.6	41.3
					3	3.73			
					3	3.45			

[a] $\varepsilon = \Sigma(k^3\chi(k)_{exp} - k^3\chi(k)_{calc})^2/\Sigma(k^3\sigma(k)_{exp})^2$.

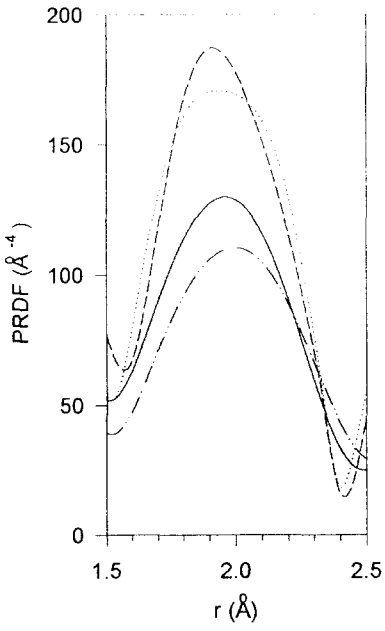

Fig. 7. First peak of the PRDF with window used: continuous line, Hanning window (3.5–13.0 Å); dashed/dotted line, Hanning window (3.0–11.0 Å); dashed line, Tournarie window (external range 3.5–13 Å, internal range 4.5–11 Å); dotted line, Tournarie (external range: 3.5–13.8 Å, internal range 4.5–13.0 Å).

the window, the peak width and height significantly change but not the peak position. The first peak position varied ±2% when distinct types of window with different width were used. A fitting of the same PRDF peak obtained using a Hanning window between 3.5 and 13.0 Å^{-1} abides by a model of sixfold coordinated Y and $R_1 = 2.54$ Å with $\varepsilon = 4.0$. Accordingly, we consider that it is independent of the window used within an estimated error of 2%.

For the 2C sample a one-shell model was not possible. Only when a second shell was included at the distance of the Y–O bond length usually found in zirconia–yttria solid solutions [34,35] (2.33 Å), was a satisfactory value of the relative deviation between experimental and calculated EXAFS functions (ε) obtained. The Y-cation shell fits a three-shell model. In this case, seven parameters had to be adjusted (three bond lengths, three coordination numbers and the Debye–Waller factor). According to the Nyquist criterion [36], the number of parameters P that can be obtained from the EXAFS measurement is given by $P = (2\Delta R\Delta k)/\pi$, where Δk is the range to calculate the FT and ΔR is the range of R space where the inverse transformation was performed. Accordingly, the number of parameters is $P = (2 \times 8 \times 1.5)/\pi = 7.6$.

Before calcination, the powder XRD pattern (Fig. 8) presents the characteristic broad peaks of amorphous materials. After calcination, the three possible polymorphs at atmospheric pressure (cubic, tetragonal and

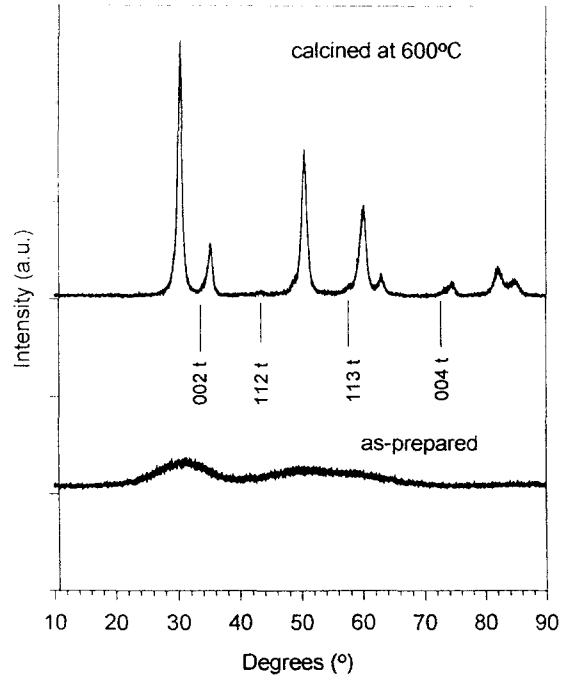

Fig. 8. X-ray diffraction patterns of as-prepared (dotted line) and calcined (continuous line) zirconia powders doped with yttria at 6 mol%.

monoclinic) can be detected. The (112), (002), (113) and (004) reflections of the t-ZrO_2 phase can be observed. The monoclinic phase concentration, calculated with the formula of Garvie et al. [37] is 7.7%.

4. Discussion

The Zr K-edge PRDF of as-prepared sample presents a first peak higher than that of the calcined sample, indicating the short-range order around Zr atoms. The Y K-edge PRDF peaks are very low, revealing an almost chaotic ordering, the arrangement around Y atoms being almost nonexistent. After heat treatment a growth of second peaks and a shortening of the Zr–O and Y–O bond lengths, caused by crystallization, are observed. The first and second peak of the Zr edge PRDF has a similar magnitude. In this type of compound the second peak amplitude decreases with increasing cubic phase concentration [18]. This is a consequence of the atomic disorder of stabilized c-ZrO_2, due to the charge compensating oxygen vacancy generated by the substitutional dopant atoms. Thus it is necessary to accommodate seven atoms in a cube, four in the vertex and three slightly shifted along the edge towards the vertex where there is an oxygen vacancy. Both cation–O shells have similar amplitudes, while the Y-cation shell is larger and has higher amplitude than the Zr-cation shell. One of the characteristics of zirconia with low yttria concentration is that the atomic arrangements around Zr and Y at the second nearest neighbor level are indistinguishable [19]. However, by back transforming the second shell contributions (Fig. 9), remarkable differences between the second shells of both cations are observed, implying a considerable inhomogeneity.

The Zr–O shell of 1C sample fits a single shell at 2.22 Å × 8, the starting parameters. The best fit to the Zr–O shell of the calcined sample gives a shorter bond length (2.18 Å) and fourfold coordination. This bond length agrees with the reported values because in our sample all the polymorphs are present and, therefore, an average value near to the bond length of the majority phase is to be expected. The low coordination number obtained can be attributed to a two-shell structure of ZrO_8 units in which the outer Zr–O subshell cannot be seen at room temperature because it corresponds to loose Zr–O bonds. They contribute only to a broad background of the X-ray absorption spectrum. The next nearest neighbors' shell presents a small deviation from the values expected for the reported yttria stabilized cubic zirconia (12×3.62Å) [19].

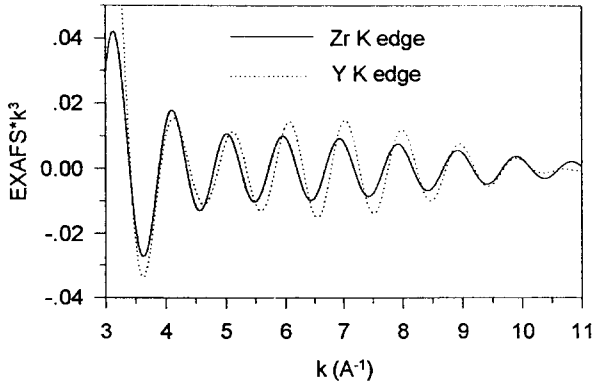

Fig. 9. Fig. 5 EXAFS spectra for Zr-cation shell (continuous line) and Y-cation shell (dotted line) in calcined zirconia powders doped with yttria at 6 mol%.

Concerning the Y K-edge analysis, the high resulting Debye–Waller factor indicates the chaotic arrangement around the Y atoms in the 1C sample. The value of R_1 is 10% larger than Y–O bond distance in Y_2O_3 and those found for yttria doped zirconia by, for example Ping-Li et al. [19]. However, the Zr–O bond lengths are in agreement with the results reported in this paper. This means that before calcination Y atoms have not merged with the zirconia network but form very small particles of a separate phase, probably consisting of distorted $Y(OH)_3$ units. These particles are so small that scanning electron micrography, performed with × 40 000 magnification, cannot resolve them [38]. This is fine enough to consider the elongation of Y–O bonds caused by the surface effect. We attribute this structural difference, with regard to the samples studied by those authors, to the processing. In our case Y is introduced as raw Y_2O_3, while those authors feature samples in which the Y was taken from different salts. In our samples the Y atoms join the zirconia network during the thermal treatment. After calcination part of the Y has been incorporated into the zirconia network. The results of the 2C sample indicate that only a fraction of Y atoms form a part of the yttria–zirconia solid solution network. This is corroborated by the complex fitting of the second-nearest neighbor shell which does not fit a single frequency filtered EXAFS function.

5. Conclusions

The three zirconia polymorphs at atmospheric pressure coexist in the calcined sample in which the cubic cells are very distorted, as indicated by the apparent low coordination number of the Zr atom.

The Y K-edge filtered EXAFS signal of the 1C sample neither fits the standard values reported in the literature for zirconia–yttria solid solutions, nor that of Y–O in Y_2O_3. The Y atoms are not mixed with the Zr atoms at all. However, 25% of the Y atoms of the calcined sample may be integrated in the network;

hence the powders must be considered inhomogeneous. The second nearest neighbor analysis also indicated important inhomogeneities at an atomic level.

Acknowledgements

The authors thank the staff in charge of D.C.I. machine for allocation of the beam time. We acknowledge the Comisión Interministerial de Ciencia y Tecnología (Acción Especial MAT-90-1153/E) Junta de Andalucía (exp. no. 6015) and Ministerio de Educación y Ciencia for the financial support of this work.

References

[1] L.C. Klein, in L.C. Klein (ed.), *Sol–Gel Technology for Thin Films, Fibers, Preforms, Electronics, and Specialty Shapes*, Noyes, Park Ridge, NJ, 1988.

[2] M.T. Hernández, M. Osendi and J.R. Jurado, in P.Durán and J.F. Fernández (eds.), *Third Euroceramics, Faenza Editrice Ibérica, S.L. Castellón de la Plana, Spain, 1993*, Vol. 2, p. 299.

[3] I. Cañadilla, J.D. Solier and A. Domínguez-Rodríguez, in P.Durán and J.F. Fernández (eds.), *Third Euroceramics, Faenza Editrice Ibérica, S.L. Castellón de la Plana, Spain, 1993*, Vol. 2, p. 259.

[4] C. Combescure, A. Sabri, C. Labatut, D. Thenegal and B. Armas, in P.Durán and J.F. Fernández (eds.), *Third Euroceramics, Faenza Editrice Ibérica, S.L. Castellón de la Plana, Spain, 1993*, Vol. 2, p. 787.

[5] E. Blachere, P. Chainiau and E. Beauprez in P.Durán and J.F. Fernández (eds.), *Third Euroceramics, Faenza Editrice Ibérica, S.L. Castellón de la Plana, Spain, 1993*, Vol. 2, p. 721.

[6] W.F. Doyle, B.D. Fabes, J.C. Root, K.D. Simmons, Y.M. Chiang and D.R. Uhlmann, in J.D. Mackenzie and D. Ulrich (eds.), Ultrastructure Processing of Advanced Ceramics, Wiley, New York, 1988, p. 953.

[7] A.C. Pierre, Sol–gel processing of ceramic powders, *Ceram. Bull., 70* (8) (1991) 1281.

[8] K. Haberko, Characteristics and sintering behaviour of zirconia ultrafine powders, *Ceremurgia Int., 5* (4) (1979) 148.

[9] B. Fegley, P. White and H.K. Bowen, Processing and characterization of ZrO_2 and Y-doped ZrO_2 powders, *Am. Ceram. Soc. Bull., 64* (8) (1985), 1115.

[10] G.F. Tu, Z.T. Sui, Q. Huang and Ch.Z. Wang, Sol–gel processed Y–PSZ ceramics with 5 wt.% Al_2O_3, *J. Am. Ceram. Soc., 75* (4) (1992) 1032.

[11] K.S. Mazdiyasni, C.T. Lynch and J.S. Smith, Preparation of ultrahigh purity submicron refractory oxide, *J. Am. Ceram. Soc., 48* (7) (1965) 372.

[12] E. Tani, M. Yoshimura and S. Somiya, Hydrothermal preparation of ultrafine monoclinic ZrO_2 powder, *J. Am. Ceram. Soc., 64* (12) (1981) C-8.

[13] M.A. Blesa, A.J.G. Maroto and S.I. Passagio, Hydrous zirconium dioxide: interfacial properties, the formation of monodisperse spherical particles, and its crystallization at high temperatures, *J. Mater. Sci., 20* (1985) 4601.

[14] E. Matijevic, A. Bell, R. Brace and P. McFadyen, formation and surface characteristics of hydrous metal oxide sols, *J. Electrochem. Soc., 129* (7) (1973) 893.

[15] G. Rinn and H. Schmidt, Preparation of Y-doped zirconia by emulsion technique, in H. Hausner, G.L. Messing and S. Hirano (eds.), *Ceramic Powder Processing Science*, Köln, Germany, 1989, p. 221.

[16] R. Stevens (ed.), *Zirconia and Zirconia Ceramics*, Magnesium Elektron, Ltd.

[17] H.G. Scott, Phase relationships in the zirconia–yttria systems, *J. Mater. Sci., 10* (1975) 1527.

[18] P. Li, I.-W. Chen and J.E. Penner-Hahn, *Phys. Rev. B, 48* (1993) 10063.

[19] P. Li, I.-W. Chen and J.E. Penner-Hahn, *Phys. Rev. B, 48* (1993) 10074.

[20] P. Li, I.-W. Chen and J.E. Penner-Hahn, *Phys. Rev. B, 48* (1993) 10082.

[21] C. Prieto, P. Lagarde, H. Dexpert, V. Briois, F. Villain and M. Verdaguer, *Meas. Sci. Tech., 3* (1992) 325.

[22] K. Teo, *EXAFS: Basic Principles and Data Analysis in Inorganic Chemistry Concepts 9*, Springer Verlag, Berlin, 1986.

[23] A.G. Mckale, B.W. Veal, A.P. Paulikas, S.K. Chan and G.S. Knapp, *J. Am. Chem. Soc., 110* (1986) 3763.

[24] J.J. Rehr, J. Mustre de León, S.I. Zabinsky and R.C. Albers, *J. Am. Chem. Soc., 113* (1991) 5135.

[25] D.K. Smith and H.W. Newkirk, *Acta Crystallogr., 18* (1965) 983.

[26] O. Othaka, T. Yamanaka, S. Kume, N. Hara, H.Asano and F. Izumi, *Proc. Jpn. Acad. B, 66* (1990) 193.

[27] G. Teufer, *Acta Crystallogr., 15* (1962) 1187.

[28] P. Alderbert and J.P. Traverse, *J. Am. Ceram. Soc., 68* (1985) 34.

[29] D. Michel, L. Mazerolles and M. Pérez y Jorba, *J. Mater. Sci., 18* (1983) 2618.

[30] D. Steele and B.E.F. Fender, *J. Phys. C, 7* (1974).

[31] D.K. Smith and C.F. Cline, *Am. Ceram. Soc., 45* (1962) 249.

[32] A.N. Christensen, R.G. Hazell and Å. Nilsson, *Acta Chem. Scand., 21* (1967) 481–492.

[33] R.D. Shannon, *Acta Crystallogr. A, 32* (1976) 751.

[34] M.H. Tuilier, J. Dexpert-Ghys, H. Dexpert and P. Lagarde, *J. Solid State Chem., 69* (1986) 272.

[35] C.R.A. Catlow, A.V. Chadwick, G.N. Greaves and L.M. Moroney, *J. Am. Chem Soc., 69* (1986) 272.

[36] E.O. Brighm, in *The Fast Fourier Transform*, Prentice-Hall, New York, 1971.

[37] R.C. Garvie, R.H. Hannick and R.T. Pascoe, Ceramic Steel, *Nature, 258* (5537) (1975) 703–704.

[38] C. Barrera-Solano, C. Jiménez-Solís, N. de la Rosa-Fox and L. Esquivias, in P.Durán and J.F. Fernández (eds.), *Third Euroceramics, Faenza Editrice Ibérica, S.L. Castellón de la Plana, Spain, 1993*, Vol. 1, p. 721.